

Tailoring poly(vinylidene fluoride – co - chlorotrifluoroethylene) microstructure and physico-chemical properties by exploring its binary phase diagram with dimethylformamide

Ricardo E. Sousa^{1a}, José Carlos C. Ferreira^{1a}, Carlos. M. Costa¹, Ana V. Machado², Maria M. Silva³, Senentxu Lanceros-Mendez¹

¹Departamento/Centro de Física, Universidade do Minho Campus de Gualtar, 4710-057 Braga, Portugal

²IPC – Institute for Polymers and Composites, Universidade do Minho, Campus de Azurém, 4800-058 Guimarães, Portugal

³ Departamento/Centro de Química, Universidade do Minho Campus de Gualtar, 4710-057 Braga, Portugal

^aThese authors contributed equally

Correspondence to: S. Lanceros-Mendez (E-mail: lanceros@fisica.uminho.pt)

((Additional Supporting Information may be found in the online version of this article.))

ABSTRACT

Poly(vinylidene fluoride-co-chlorotrifluoroethylene), PVDF-CTFE, membranes were prepared by solvent casting from dimethylformamide, DMF. The preparation conditions involved a systematic variation of polymer/solvent ratio and solvent evaporation temperature. The microstructural variations of the PVDF-CTFE membranes depend on the different regions of the PVDF-CTFE/DMF phase diagram, explained by the Flory-Huggins theory. The effect of the polymer/solvent ratio and solvent evaporation temperature on the morphology, degree of porosity, β -phase content, degree of crystallinity, mechanical, dielectric and piezoelectric properties of the PVDF-CTFE polymer were evaluated. In this binary system, the porous microstructure is attributed to a spinodal decomposition of the liquid-liquid phase separation. For a given polymer/solvent ratio, 20 wt%, and higher evaporation solvent temperature, the β -phase content is around 82% and the piezoelectric coefficient, d_{33} , is - 4 pC/N.

KEYWORDS: PVDF-CTFE, membranes, thermal induced phase separation, phase diagram

INTRODUCTION

Fluoropolymers are a class of polymers with increasing interest due to their wide range of actual and potential applications¹.

In particular, they are being used for aerospace applications^{2,3}, gaskets, seals, petrochemical, automotive, medical and electrical industries³, lubricants, thermal insulators, chemically resistant materials, filter membranes and as electrical insulators². Potential applications include energy storage and advanced electronic devices begin explored due to the electroactive properties of some fluoropolymers⁴.

Among their most interesting properties are chemical, thermal^{2,3,5} and electrical stabilities, inertness to acids, high resistance to aging and oxidation^{2,3}, low refractive index, low or no flammability³ and mechanical strength.

On the other hand, some characteristics such as their highly hydrophobic and solvophobic nature leading to poor solubility, wettability and miscibility with other materials, limit their applications in fields such as filtration membranes and medical devices².

In this way, strong research efforts have been developed to tune materials properties by varying the chemical compositions and therefore to extend their application range. Fluoropolymers that contain certain functional groups such as tetrafluoroethylene (TFE) and hexafluoropropene (HFP) have been developed by direct copolymerization with functional fluoro-monomers or by modification of fluoropolymers without any functional groups^{1,2,4,6}. One of these fluoropolymers is the poly(vinylidene fluoride-co-chlorotrifluoroethylene) (PVDF-CTFE) copolymer.

PVDF-CTFE copolymers with small VDF content are semicrystalline copolymer with a hexagonal structure^{4,7}. The copolymers with high VDF content (containing 25-70 mol% VDF) are semicrystalline with a monoclinic crystalline structure⁴ and can be also obtained in the amorphous state.

PVDF-CTFE copolymer shows the $[(CH_2CF_2)_x(CF_2CFCl)_y]_n$ ^{4,7} chemical structure,

the relative CTFE content being critical in determining the copolymer physico-chemical properties⁷. In particular, there is a strong influence on the thermal properties, the glass transition temperature, T_g , ranging from ~ -40 °C (for pure PVDF) to 45 °C for PCTFE⁷.

Ferroelectric PVDF and its copolymers (PVDF-CTFE) show strong dipolar moments originating from the C-F bonds, the orientation of dipoles in the crystalline phase being responsible for the piezoelectric properties⁸. A high electromechanical response is reported for PVDF-CTFE^{4,7} containing 9 and 12 mol.% CTFE⁷ and its dielectric permittivity is 13 and dependent on CTFE content. The first applications of PVDF-CTFE were wire and cable covers due to its high flexibility, high elongation and cold impact resistance. Nowadays, this polymer also begins to find applications in membranes for water and organic liquid treatment¹ and non-volatile polymer memories⁹. The pseudo-block structure of PVDF-CTFE offers feasibility for possible grafting modification via atom transfer radical polymerization (ATRP) preserving the high mechanical, thermal and chemical stabilities⁵. Nowadays strong research efforts are being develop on the use of the materials for electrical energy storage⁹⁻¹², as high energy material³ and the development of gel electrolyte membranes containing. In particular, its key features for energy storage application are its high ionic conductivity and good compatibility with lithium metal electrodes⁶.

CTFE is also used in ternary polymers with VDF and TrFE (trifluoroethylene) or HFP to further tune electromechanical transduction and dielectric permittivity, etc^{6,7,13}. In the terpolymers, the CTFE units disrupts the sequence length of the crystal, which lowers both the melting and Curie transitions leading to good electromechanical response through the more mobile polar domains¹³. The presence of the chlorine atom in the terpolymers of VDF and TrFE imposes a larger steric hindrance, which favors the (ferroelectric) trans conformation of the polymer backbone¹³. The addition of CTFE to the VDF-HFP copolymer has

the effect of increasing the melting point and increasing the amorphous content ⁶.

Several techniques have been used for the processing of P(VDF-CTFE) membranes, including solution casting ^{2,4,13}, electrospinning ^{12,14} and non-solvent induced phase inversion ⁵. Terpolymer films have been produced from solvent/non-solvent systems ⁶ and spin-coating ⁹ but there is still a need to establish clear processing-morphology-physical properties relationships for this important copolymer, in particular for the development of polymer membranes.

Taking into account the state of art for PVDF-CTFE membranes and the need of understanding and tailoring its microstructure for different applications, the novelty of this work is the fabrication of PVDF-CTFE membranes by solvent casting from N,N-dimethylformamide (DMF), by varying systematically polymer concentration and evaporation temperature along the phase diagram of the polymer/solvent system. Thus, membranes with different microstructures have been obtained with distinct thermal, mechanical, dielectric and piezoelectric properties, suitable for a wide range of applications.

EXPERIMENTAL

Materials

Poly(vinylidene fluoride-co-chlorotrifluoroethylene) PVDF-CTFE (Solef 31508 with Mw = 270-290 kg/mol; 18.66wt% of CTFE content ¹⁵) was supplied by Solvay. The solvent N, N-dimethylformamide (DMF, 99.5%) was purchased from Merck.

Membrane preparation

PVDF-CTFE polymer concentration in solution ranged from 5 wt% to 20 wt%, concentration at which the polymer showed already a large viscosity. The polymer was dissolved in DMF at room temperature under constant magnetic stirring until a homogeneous solution was

obtained. After polymer dissolution, the solution was placed on a clean glass substrate, spread by blade coating with the thickness of 100 μm and submitted to isothermal evaporation in a temperature range between 25°C and 200 °C within an air oven from Binder, ED23 oven.

The samples produced were identified as (x CTFE y) where x represent the polymer concentration and y represents the solvent evaporation temperature.

Sample characterization

The morphology of the PVDF-CTFE membranes was obtained by scanning electron microscopy (SEM) (Cambridge, Leica) with an accelerating voltage of 15 kV. Previously the samples were coated with a thin gold layer using a sputter coating (Polaron, model SC502 sputter coater). The porosity of the samples (ϕ) was measured by the pycnometer method ¹⁶:

$$\phi = \frac{W_2 - W_3 - W_s}{W_1 - W_3} \quad (1)$$

In equation 1 W_1 is the weight of the pycnometer filled with ethanol, W_s is the mass of the sample, W_2 is the weight after the sample was soaked in ethanol and additional ethanol was added to complete the volume of the pycnometer and W_3 is obtained when the sample was removed from the pycnometer and the residual weight of the pycnometer with ethanol was measured.

The mean porosity of each membrane was obtained as the average of the values determined in three samples.

Contact angle measurements (sessile drop in dynamic mode) were performed at room temperature in a Data Physics OCA20 device using ultrapure water (3 mL droplets) as the test liquid. At least 3 measurements on each sample were performed in different sample locations and the average contact angle was calculated.

Fourier Transformed Infrared spectroscopy (FTIR) was used for the identification of the polymer crystalline phase at room temperature

with a Jasco FT/IR-4100. FTIR spectra were collected in attenuated total reflectance mode (ATR) from 4000 to 600 cm^{-1} after 32 scans with a resolution of 4 cm^{-1} .

Thermal properties (melting temperature and degree of crystallinity) were determined by differential scanning calorimetry (DSC) with a Mettler Toledo 821e apparatus. The samples were cut from the central region of the membranes, placed in 40 μL crucibles and heated from 25 to 200 $^{\circ}\text{C}$ at a rate of 10 $^{\circ}\text{C}/\text{min}$, under a argon atmosphere.

Mechanical tests were carried out at room temperature through stress-strain measurements in the tensile mode of a Shimadzu-AG-IS testing instrument at a strain rate of 1mm/min

The real part of the dielectric permittivity (ϵ') and the dielectric losses ($\tan \delta$) were obtained at room temperature in the frequency range of 200 Hz to 1 MHz with an applied voltage of 0.5 V. Circular aluminum electrodes of 5 mm diameter were vacuum evaporated onto both sides of each sample.

The piezoelectric d_{33} coefficients were measured using a d_{33} meter APC YE2730A. For determination of the piezoelectric coefficient, the PVDF-CTFE samples were first poled by corona discharge at a controlled temperature inside a home-made corona chamber with the following parameters obtained after process optimization: applied voltage of 8 kV at a constant current of 10 μA ; constant distance of 1.5 cm between the sample and the tip; poling time 1 hour, poling temperature at 120 $^{\circ}\text{C}$ and then cooled to room temperature under the applied electric field¹⁷.

MESOSCALE SIMULATION

Mesosopic models based on dynamic density functional were used for describing the phase separation phenomena in the polymer/solvent mixture.

The dynamic density functional (DDF) model (mesoscale model based on the Gibbs free

energy) consists on representing the total functional free energy as a function of time. This model is represented by the diffusion equation of the time-dependent Ginzburg-Landau model¹⁸:

$$\frac{\partial \phi(r,t)}{\partial t} = \frac{M \nabla^2 \delta F}{\delta \phi(r,t)} + \eta(r,t) \quad (2)$$

where $F = F^{id} + F^{mf}$ (F^{id} is the ideal free energy function and F^{mf} is the mean field free energy that correspond to Gibbs free energy, ϕ is the volume fraction of the polymer, M is the kinetic coefficient and $\eta(r,t)$ is a Gaussian random force, corresponding to a force correction factor¹⁸.

The simulation was executed through the MesoDyn Model of Materials Studio software v6.0.0. The MesoDyn software solves the DDF problem applied to polymer mixtures by varying volume fraction and temperature, in order to assess the conditions for crystallization nucleation to occur. Within this process, it was necessary to build a polymer chain of PVDF-CTFE and a DMF molecule. Further, it was required to build an amorphous cell of polymer mixture based on the polymer-solvent volume fractions corresponding to the ones established in the experimental work. Finally, the polymer phase separation was studied as a function of the polymer concentration within the solution and the solvent evaporation temperature independently of the size of the box¹⁹. The size of the box was 502x502x32 nm with a number of simulation steps of 2000.

RESULTS

Morphology, degree of porosity and contact angle

The microstructural variations observed through the SEM images obtained from the P(VDF-CTFE)/DMF binary system with DMF by varying initial polymer concentration (5 to 20

wt%) and solvent evaporation temperature (25°C to 200°C) are shown in figure 1.

As a function of initial polymer concentration (figure 1a, 5wt% and 1b, 20wt%) at 25°C, it is observed a porous morphology formed by sponge-like macrovoids as a result from a precipitation situation dominated by liquid-liquid demixing in the phase diagram²⁰. This behavior is explained through the phase diagram of the figure 9b, as it will be discussed later. A porous morphology is also observed in the samples prepared after solvent evaporation at 50°C (figure 1c, 5wt% and 1d, 20wt%)

For low solvent evaporation temperatures (25°C and 50°C) at a given polymer concentration (5 wt%) - figure 1 a) and c) - the membranes are characterized by a uniformly distributed spherulitic particulate morphology. Figure 1 a) and c) also show that the size of the spherulites increases with increasing solvent evaporation temperature. This behavior is the same independently of the polymer concentration in the solution, as shown by figures 1b) and d) for the 20 wt% samples concentration. Moreover, for a given polymer concentration, the size of the spherulites increases with increasing of solvent evaporation temperature (figures 1b and 1d).

The particular morphology observed in figures 1 a-d) is ascribed to the relevance of the amorphous fraction in the formation of the membrane at lower crystallization temperatures (25°C and 50°C). At these temperatures, the amorphous phase supplies sufficient chain mobility through to reorganize the membrane structure, which is interrupted

at the time of polymer vitrification²¹, leading to low values of degree of crystallinity (table 2).

A different microstructure is observed at high solvent evaporation temperatures for the 20wt% sample. As observed in figure 1e and figure 1f) for solvent evaporation at 100°C and 200°C, the membranes exhibit a dense morphology as temperature improves the polymer diffusion and the spherulite growth due to increased mobility of the polymer chains, that occupy the free space left by the solvent, giving rise therefore to a dense morphology²².

The pores observed in figure 1e) for the samples evaporated at 100°C are the result of the high evaporation rate of the DMF solvent that limits the mobility of polymer chains (see the phase diagram in the discussion section).

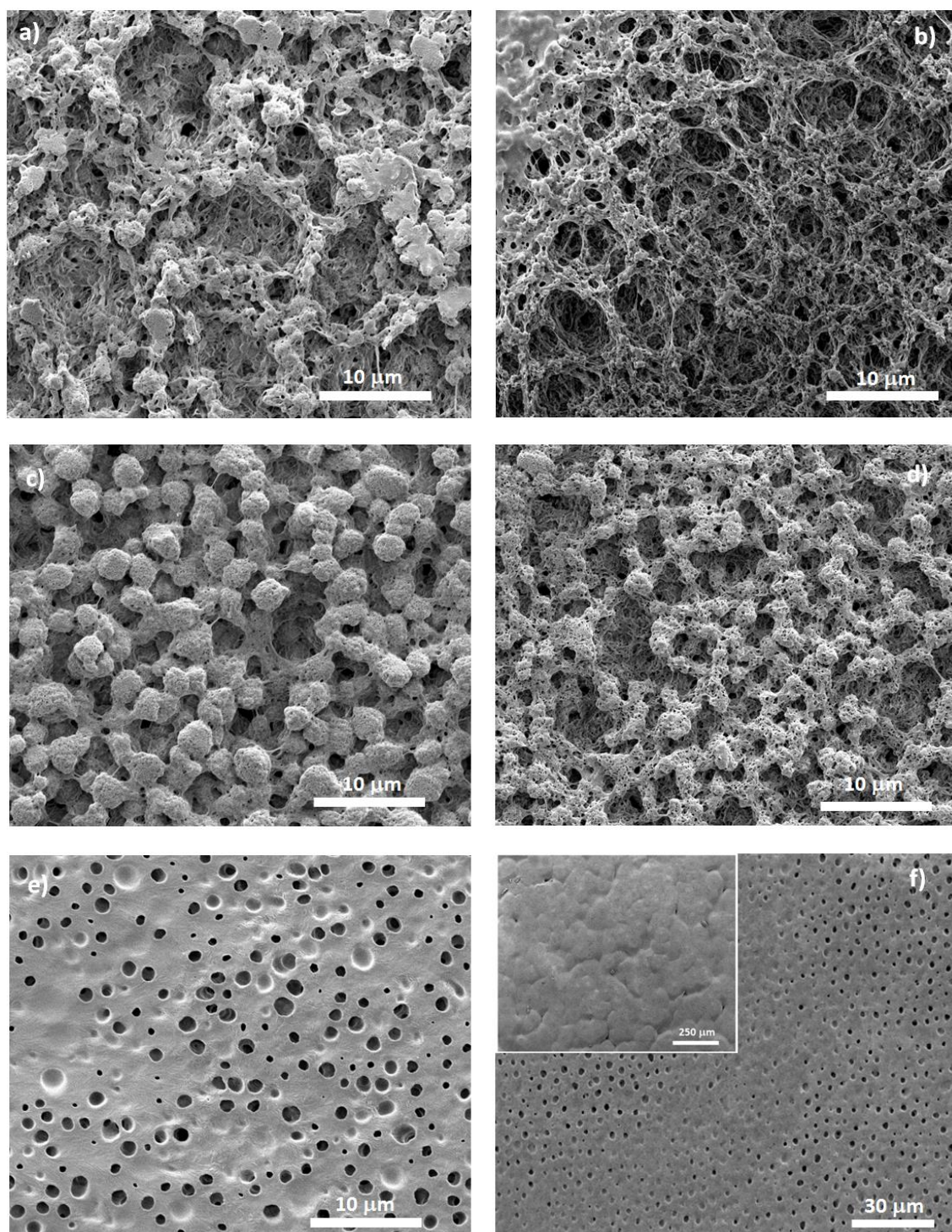


FIGURE 1 Surface images of the PVDF-CTFE membranes prepared from the PVDF-CTFE/DMF solution: solvent evaporation at 25°C for 5 wt% PVDF-CTFE (a) and 20 wt% PVDF-CTFE (b) samples. Solvent evaporation at 50°C for a 5 wt% PVDF-CTFE (c) and 20 wt% PVDF-CTFE samples (d). Morphologies of the samples with 20 wt% PVDF-CTFE with solvent evaporation at 100 °C (e) and 200 °C (f).

The morphology observed for the samples evaporated at 200°C (figure 1f) consist on thick films with just surface pores within spherulites of diameters around 100 μm (insert of figure 1f).

The different morphologies shown in figure 1 are attributed to the initial position of the solution in the phase diagram of the PVDF-CTFE/DMF system (see later, figure 9b). The evaporation temperature of the solvent and the PVDF-CTFE concentration strongly affects the membrane morphology and the degree of porosity (figure 2).

Figure 2 represents the degree of porosity of the PVDF-CTFE membranes evaporated at 25°C as a function of the initial polymer concentration. The degrees of porosity ranges between 70 % and 60 % for all initial polymer concentrations in the solution between 5 and 20 wt%.

The explanation of this morphology is the low evaporation temperature, the polymer chains have a reduced mobility hindering the polymer to occupy the free space left by the evaporated solvent ²³.

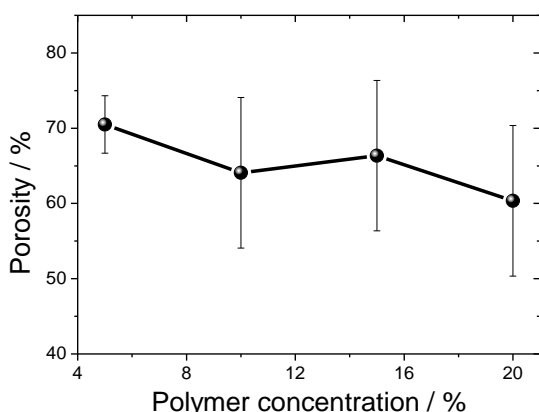


FIGURE 2 Degree of porosity as a function of PVDF-CTFE initial concentration in the PVDF-CTFE/DMF system prepared by solvent evaporation at room temperature.

This behavior at 25°C also is detected for PVDF-CTFE membranes evaporated at 50°C, the degree of porosity ranging, in this case,

between 56 % and 40 % for 5 and 20 wt% of PVDF-CTFE in the initial solution, respectively.

The decrease in degree of porosity for PVDF-CTFE membrane evaporated at 50°C and 100°C in comparison with sample at 25°C for a given polymer concentration (e.g. 5 wt%) is due of the increased of solvent evaporation rate and increased polymer chain mobility ²⁴.

For higher solvent evaporation temperature at 200°C, a thick film is observed with no porosity. It is to notice that the evaporation temperature is above the melting temperature of the copolymer and under this temperature conditions, and different from the other situations, melt crystallizations occurs. The analysis of the hydrophobicity of the membranes is essential to determine their range of applicability. Figure 3 shows the contact angle as a function of initial polymer concentration for the different solvent evaporation temperatures.

For PVDF-CTFE membranes evaporated at 25°C the water contact angle is approximately between 130° and 140°, independently of the initial polymer concentration. The hydrophobic character observed for these membranes is mainly related to the large pore size and irregular surface ²⁵.

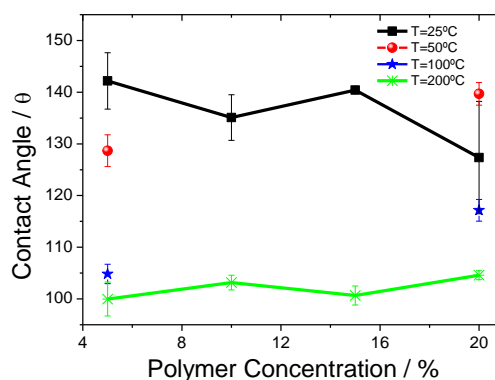


FIGURE 3 Contact angle as a function of PVDF-CTFE initial polymer concentration in the solution and the different evaporation temperatures.

In a general way, the water contact angle decreases with increasing solvent evaporation

temperature, as shown in Figure 3 for the 5 wt% initial polymer concentration, suffering minor variations with the initial polymer concentration. Thus, for the initial polymer concentration of 5 wt% there is a strong decrease of the contact angle from $\sim 140^\circ$ to $\sim 100^\circ$ from the samples evaporated at 25 °C and 200 °C, respectively (figure 1f). This fact is mainly attributed to the variations in the morphology of the samples²⁶, but can also on the polymer phase and therefore the polarity of the polymer chains.

Infrared analysis

Typically PVDF-CTFE polymer with less than 17 mol % CTFE content crystallizes in the non-polar α -phase²⁷.

The identification and quantification of the crystalline phase of PVDF-CTFE as a function of the initial polymer concentration and solvent evaporation temperature was performed by Fourier transform infrared spectroscopy (FTIR) (figure 4).

The specific bands characteristic of the α and β -phases of the pure PVDF polymer are 765, 796, 855 and 976 cm^{-1} and 840 and 1232 cm^{-1} , respectively²⁸.

The more representative vibration bands of PCTFE co-polymer are: C-C stretch at 649, 666 and 698 cm^{-1} , C-Cl stretch at 902, 937 and 970 cm^{-1} , F-C-F asymmetrical stretch at 1202 cm^{-1} , F-C-F symmetrical stretch at 1130 cm^{-1} and C-F stretch at 1285 cm^{-1} ²⁹.

FTIR-ATR spectra for the PVDF-CTFE membranes prepared after solvent evaporation at 25 °C for different initial polymer concentration are shown in the figure 4 a). Figure 4 b) shows the FTIR-ATR spectra for the membranes prepared with the same initial polymer concentration (20 wt%) but with solvent evaporation temperature between 25 °C to 200 °C.

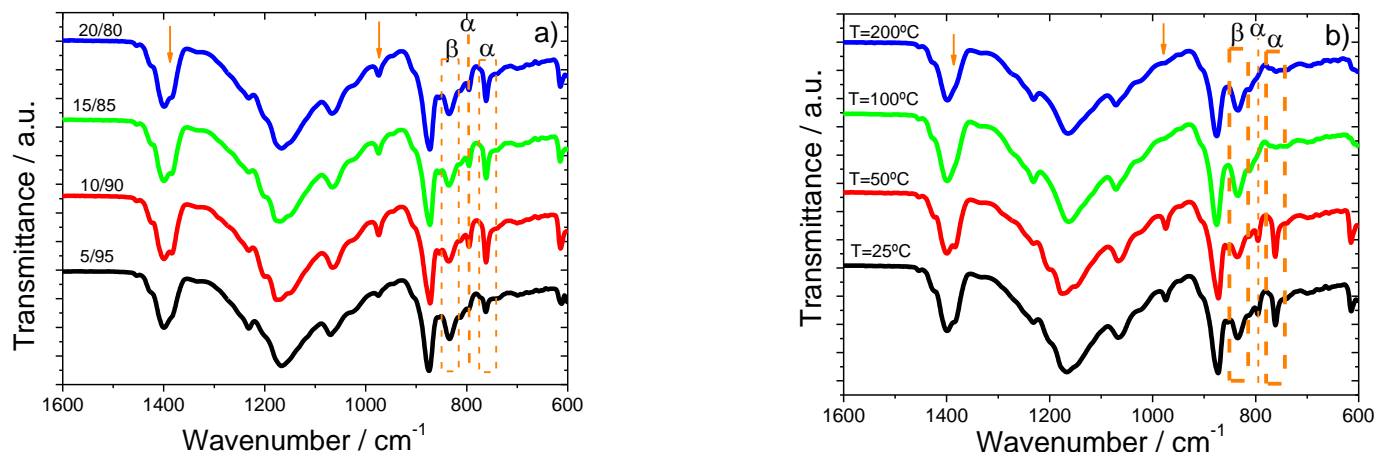


FIGURE 4 FTIR-ATR spectra for a) samples prepared after solvent evaporation at $T=25^\circ\text{C}$ for different initial polymer concentrations in the PVDF-CTFE/DMF system and b) samples prepared from 20 wt% PVDF-CTFE initial polymer concentration with solvent evaporated at different temperatures.

It can be observed that the polymer concentration (figure 4a) and solvent evaporation temperature (figure 4b) has a significant effect on vibrations bands of the PVDF-CTFE polymer and, therefore, different polymer phase contents are presented in the different samples.

Independently of the experimental conditions (figure 4), it is detected the presence of the vibrations bands at 760, 795, 974 and 1384 cm^{-1} that correspond to the α crystalline phase, but also the specific band at 838 cm^{-1} , identifying the β -phase²⁸. This fact confirms the coexistence of multiple phases of PVDF-CTFE polymer, as detected through of XRD and DSC, as a function of crystallization condition³⁰.

The quantification of the crystalline phases present in the samples was performed using the specific bands at 766 cm^{-1} and 840 cm^{-1} , identified with the presence of the α - and β -phases, respectively, and following the method explained in²⁸. Assuming the samples are composed just by the α and β phases, the β phase content is calculated by:

$$F(\beta) = \frac{X_{\beta}}{X_{\alpha} + X_{\beta}} = \frac{A_{\beta}}{(K_{\beta} / K_{\alpha})A_{\alpha} + A_{\beta}} \quad (3) \quad ,$$

where $F(\beta)$ represents the β phase content; A_{α} and A_{β} the absorbencies at 766 and 840 cm^{-1} , corresponding to the α and β phase material; K_{α} and K_{β} are the absorption coefficient at the respective wave number and X_{α} and X_{β} the degree of crystallinity of each phase. The value of K_{α} is 6.1×10^4 and K_{β} is $7.7 \times 10^4 \text{ cm}^2/\text{mol}$ ²⁸.

The β -phase fraction obtained for the different PVDF-CTFE membranes is summarized in table 1.

TABLE 1 – β -phase content of the PVDF-CTFE membranes prepared from different initial polymer concentrations and solvent evaporation temperatures.

Samples	β -phase / % \pm 2%
5CTFE25	56
10CTFE25	25

15CTFE25	32
20CTFE25	33
20CTFE50	26
20CTFE100	87
20CTFE200	82

Table 1 shows that the β -phase content decreases with increasing of polymer concentration in the PVDF-CTFE/DMF system for a given solvent evaporation temperature (25°C) and increases with increasing solvent evaporation temperature for a given initial polymer concentration (20 wt%). The observed behavior is determined by the solvent evaporation rate influencing the PVDF crystalline^{31,32} and also by the inclusion of the CTFE fraction in the PVDF polymer.

Concerning of the PVDF-CTFE membranes with different initial polymer concentration evaporated at 25°C, it was observed a decrease of the β -phase content with increasing initial polymer content up to 10 wt%, remaining then practically constant until the initial polymer concentration of 20 wt% (table 2) in that the inclusion of the CTFE fraction is the factor determining the β -phase content. This behavior also can be explained by the solvent diffusion as initial polymer concentration affects the diffusivity of the solvent and the the evaporation rate is dominated by the solvent diffusion coefficient³².

For higher polymer concentration of 20wt%, the increase of the β -phase fraction by increasing solvent evaporation temperature is related to the inclusion of CTFE in the PVDF which leads to an oriented packing of the $\text{CH}_2\text{-CF}_2$ dipoles favoring the formation of the β -phase, as reported in³³.

Thermal and mechanical analysis

The melting behavior and degree of crystallinity of the PVDF-CTFE membranes were determined by differential scanning calorimetry (DSC).

The DSC thermographs of the PVDF-CTFE membranes as a function of the initial polymer concentration and solvent evaporation temperature are shown in figure 5a) and b), respectively.

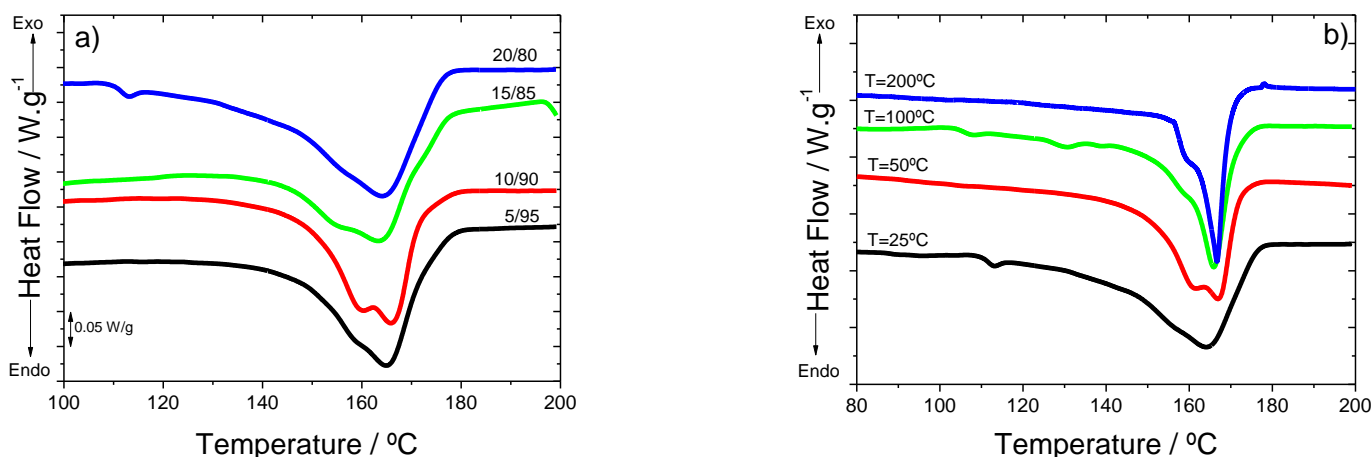


FIGURE 5 – DSC scans for a) samples prepared after solvent evaporation at $T=25\text{ }^{\circ}\text{C}$ for different initial polymer concentration in the PVDF-CTFE/DMF system and b) samples prepared from 20 wt% PVDF-CTFE initial polymer concentration with solvent evaporation at different temperatures.

Figure 5 shows in all cases a bimodal peak that represents the melting temperature of the polymer. The bimodal peak with maximum around 166°C represents the melting temperature of the PVDF-CTFE polymer⁵. Figure 5 and table 2 shows that the maximum melting temperature (164°C - 167°C) of the PVDF-CTFE membranes not is affected by the solvent evaporation temperature and polymer concentration, within experimental error. The differences observed in the bimodal peak for all PVDF-CTFE is attributed to the increase of lamellae thickness, i.e. the interlamella diffusion of the polymer chains³⁴ and the coexistence of the two crystalline phases with different crystal types

The degree of crystallinity of the PVDF-CTFE membranes, represented in Table 2, was obtained by the following equation:

$$X_c = \frac{\Delta H_m}{x(\Delta H_{100\% \text{cryst.}})_{\alpha} + y(\Delta H_{100\% \text{cryst.}})_{\beta}} \times 100 \quad (4)$$

where x is the weight fraction of the α phase, y is the weight fraction of the β phase, $(\Delta H_{100\% \text{crystalline}})_{\alpha}$ is the melting enthalpy of pure crystalline α -PVDF and $(\Delta H_{100\% \text{crystalline}})_{\beta}$ is the melting enthalpy of pure crystalline β -PVDF which is reported to be 93.04 J/g and 103.4 J/g respectively²⁸.

TABLE 2 Maximum melting temperature and degree of crystallinity of the membranes as a

function of polymer concentration and solvent evaporation temperature

Samples	Tf / °C ± 1 °C	χ / % ± 2%
5CTFE25	165	21
10CTFE25	165	21
15CTFE25	164	22
20CTFE25	164	27
20CTFE50	167	25
20CTFE100	166	15
20CTFE200	167	18

The degree of crystallinity, table 2, slightly depends on solvent evaporation temperature and initial polymer concentration.

For a given solvent evaporation temperature (25°C), the degree of crystallinity increases slightly with increasing polymer concentration due to increased polymer-polymer interaction during polymer crystallization³⁵.

On the other hand, for a given initial polymer concentration (20 wt%), the degree of crystallinity decreases with increasing solvent evaporation temperature due to increase crystallization kinetics leading to more defective structures³⁶.

It has been reported that the degree of crystallinity for PVDF-CTFE with 9wt% CTFE

content is around 25%, the degree of crystallinity decreasing with increasing CTFE content in the PVDF-CTFE polymer⁴.

The determination of the mechanical properties of the PVDF-CTFE films and membranes is a relevant factor associated to the integrity and safety of the membranes, which is critical in certain applications such as filtration, microelectronics applications and battery separators, among others.

Stress/strain curves for the different PVDF-CTFE membranes as a function of initial polymer concentration and solvent evaporation temperature are shown in Figure 6. The behavior in the stress/strain curve for all PVDF-CTFE membranes is typical for a thermoplastic polymer in which an elastic linear region characterized by the Young modulus (slope of stress-strain in the elastic region at a deformation of 5%) is detected followed by the yielding strain/stress, separating the elastic from the plastic region³⁷.

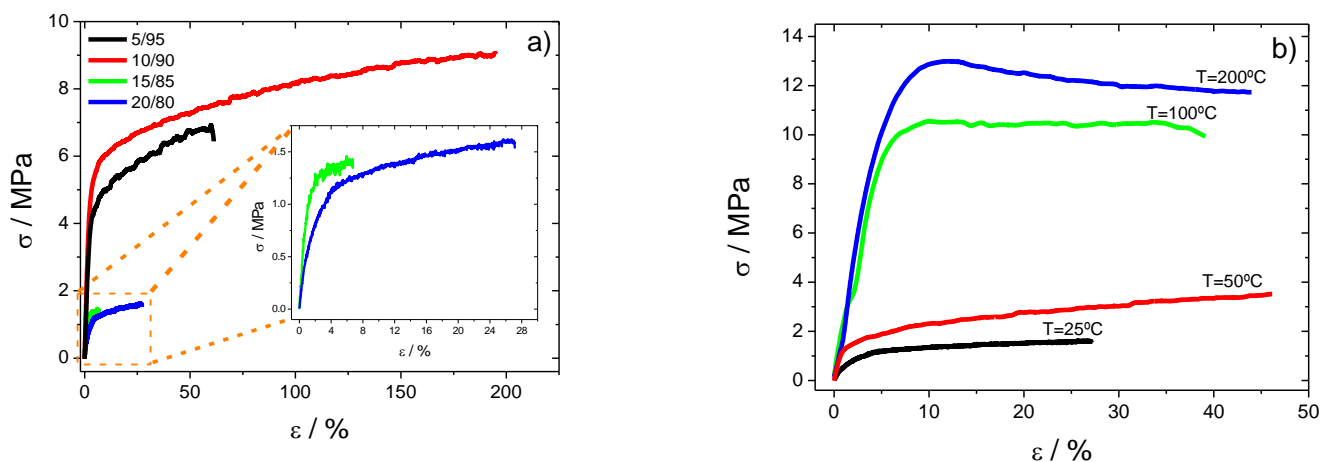


FIGURE 6 – Stress-strain curves for a) samples prepared after solvent evaporation at T=25 °C for different initial polymer concentration in the PVDF-CTFE/DMF system and b) samples prepared from 20 wt% PVDF-CTFE initial polymer concentration with solvent evaporation at different temperatures.

The mechanical parameters (Young's modulus, yielding stress/strain) calculated from the data in figure 6 are represented in table 3.

TABLE 3 Young's modulus (E'), Yielding stress (σ_y) and Yielding strain (ϵ_y) of the membranes as a function of polymer concentration and solvent evaporation temperature

Samples	$E' / \text{MPa} \pm$	$\epsilon_y / \% \pm$	$\sigma_y / \text{MPa} \pm$
	2%	1%	2%
5CTFE25	155	3	5.0
10CTFE25	155	5	6.0
15CTFE25	100	3	1.3
20CTFE25	38	4	1.2
20CTFE50	110	2	1.8
20CTFE100	180	6	10.4
20CTFE200	230	11	13

Figure 6 and table 3 show that the Young modulus and yielding stress decrease with increasing polymer concentration at 25°C. This behavior is fully ascribed to the different porous morphologies of the PVDF-CTFE membranes, as the degree of crystallinity is practically constant for those samples (table 2).

In relation to the effect of the solvent evaporation temperature, both Young modulus, yielding stress and yielding strain are enhanced with increasing solvent evaporation temperature for a given initial polymer concentration: as the solvent temperature increases, the degree of porosity present in the PVDF-CTFE membranes decreases, increasing the mechanical properties.

Dielectric and piezoelectric properties for non-porous films

Technological developments based on the use of electroactive polymers such as PVDF-CTFE are mainly based on its dielectric and piezoelectric properties, in particular for applications as sensors, actuators, electromechanical and acoustic transducers.

Figure 7 a) shows the variation of ϵ' for the PVDF-CTFE membranes evaporated at 200°C as a function of polymer concentration. These measurements are presented just for the samples prepared under these conditions, as they are processed in the form of thin films and not porous microstructures, which hinder precise electrical characterization.

ϵ' decreases with increasing frequency such as for pure PVDF³⁸ and the behavior is practically the same between all the samples.

The dielectric constant ϵ' present in the figure 7 a) is correlated and depends on the degree of crystallinity and the crystalline phase of the polymer (tables 1 and 2).

The dielectric constant ϵ' at 1 kHz as a function of polymer concentration represented in figure 7d shows the effect of the crystalline phase and degree of crystallinity in the dielectric behavior. The values of ϵ' for the PVDF-CTFE films shown in figure 7a) and 7d) are between the values of the dielectric constant obtained for the PVDF homopolymer in the α , $\epsilon' = 7$, and β -phases, $\epsilon' = 12$ ³⁸. The values of ϵ' for PVDF-CTFE polymer depend on the CTFE content and processing conditions, being reported values up to $\epsilon' = 15$ ³⁹. Figure 7 b) shows the behavior of the $\tan \delta$ as a function of frequency.

Regarding $\tan \delta$ (figure 7b) for frequencies above 10^4 Hz, the increase in the $\tan \delta$ is attributed to the α_a relaxation process, i.e, micro-brownian movement of the amorphous phase chain segments or movement of crystalline-amorphous interphase chain segments⁴⁰.

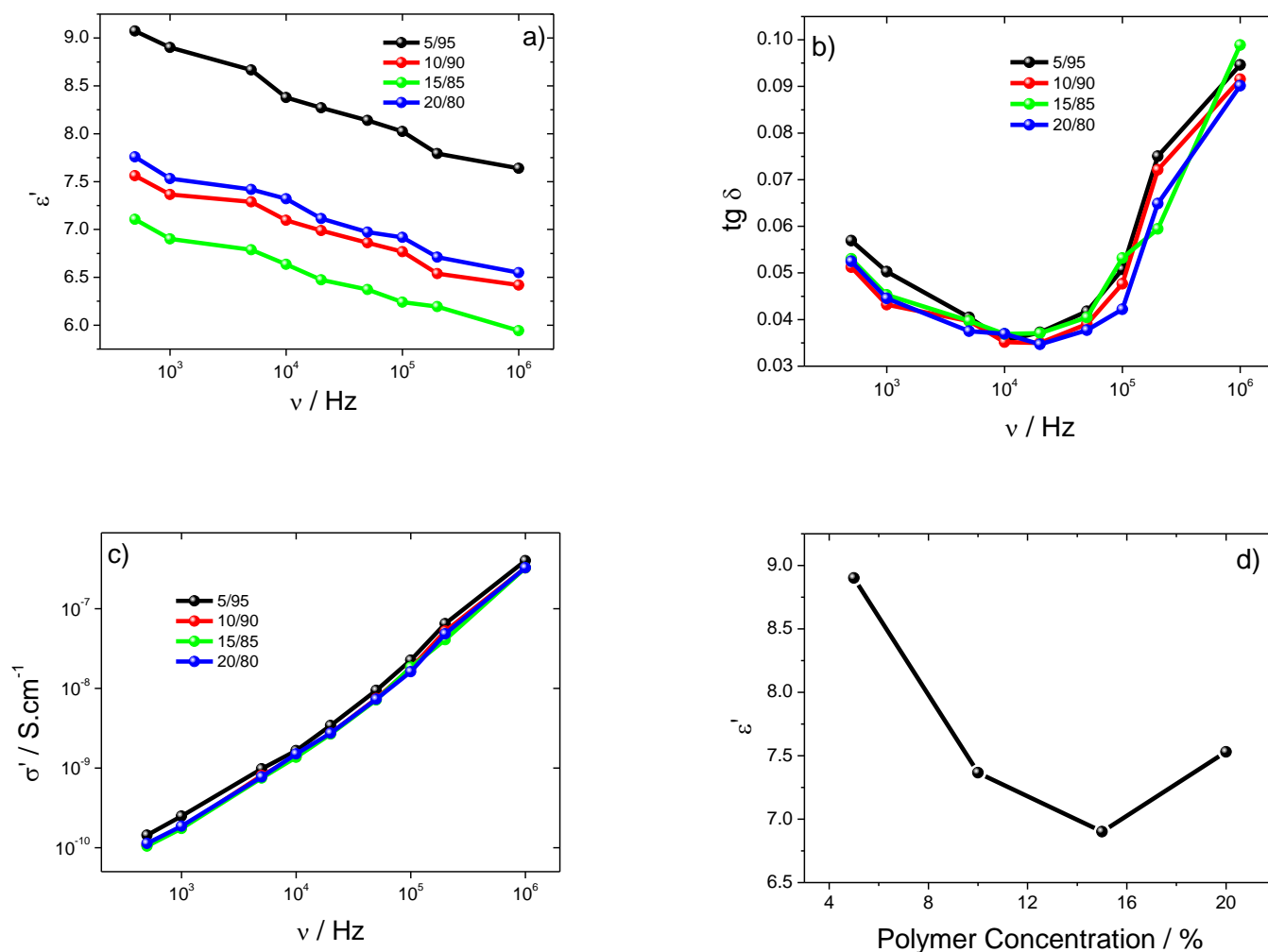


FIGURE 7 Electrical results for the samples prepared by solvent evaporation at T=200 °C from different initial polymer concentrations in the PVDF-CTFE/DMF system: a) dielectric constant, b) $\tan \delta$ and c) conductivity. d) Variation of the dielectric constant in function of polymer concentration at 1 kHz.

The real part of the conductivity of the dielectric material can be calculated from the dielectric measurements presented in Figure 6 a) after Equation 3:

$$\sigma'(\omega) = \epsilon_0 \omega \epsilon''(\omega) \quad (5)$$

where ϵ_0 is the permittivity of free space, $\omega = 2\pi f$ is the angular frequency and $\epsilon''(\omega) = \epsilon' \tan \delta$ is the frequency dependent imaginary part of the dielectric permittivity⁴¹.

Figure 7c) shows the $\sigma'(\omega)$ values for the PVDF-CTFE films as a function of frequency. The

behavior of all PVDF-CTFE films is the same, the conductivity increasing with increasing frequency (figure 7c)). Normally in the fluorinated polymers (PVDF polymer and its copolymers), the conductivity behavior as a function of frequency shows two regimes, i.e., one regime for lower frequencies up to 10^4 Hz dominated by the dc conductivity and the second for higher frequencies, assigned to the ac conductivity⁴². In the figure 7c), for all PVDF-CTFE films, the conductivity increases with increasing of frequency in a similar way.

Finally, figure 8 shows the d_{33} piezoelectric coefficient as a function of polymer concentration after poling conditions optimization.

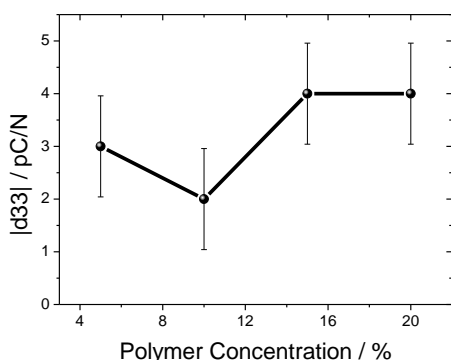


FIGURE 8 Modulus of the piezoelectric d_{33} coefficient for the films evaporated at 200 °C as a function of the PVDF-CTFE initial concentration.

The piezoelectric coefficient d_{33} is negative and the modulus of the piezoelectric d_{33} coefficient is practically independent, within experimental error, of the polymer concentration in the PVDF-CTFE/DMF system, as demonstrated in Figure 8.

In ⁴³ it is demonstrated the dependence of the piezoelectric response with the β -phase content and it was shown that for β -phase contents above 82% the piezoelectric response practically remains constant.

The piezoelectric d_{33} coefficient is around 4pC/N for the sample with the highest β -phase content (20 w%, 82%). The β -phase of the samples is responsible for the piezoelectric properties ($-\text{CH}_2\text{CF}_2-$) ⁴³ and the degree of crystallinity. In the present case, though large values of electroactive phase are obtained, the low value of the degree of crystallinity in comparison with PVDF (25% to 18% for PVDF-CTFE vs 40% to 55% for PVDF) leads to lower values of the d_{33} response ⁴⁴.

DISCUSSION

The influence of polymer concentration and solvent evaporation temperature in the sample microstructure of the PVDF-CTFE polymer (figure 1) is due to a phase separation process between polymer and solvent illustrated in the phase diagram of the PVDF-CTFE/DMF system (figure 9b).

Through of the Flory-Huggins theory based on a lattice model that ignores “free volume”, the Gibbs free energy fluctuations in the isothermal evaporation process for binary systems (polymer/solvent) are described by ⁴⁵:

$$\frac{\Delta G}{RT} = \frac{\phi}{n} \ln \phi + (1-\phi) \ln(1-\phi) + \chi_{12} \phi(1-\phi) \quad (6)$$

where n is the degree of polymerization, ϕ is the polymer volume fraction and χ_{12} is the Flory-Huggins parameter for a binary mixture.

The Flory-Huggins parameter χ_{12} in order to temperature is expressed as:

$$\chi_{12} = \frac{v_0}{RT} \delta^2 \quad (7)$$

where R is the gas constant, v_0 the molar volume of the solvent, T the temperature, and δ the Hansen solubility parameter.

For the PVDF-CTFE/DMF system, the Gibbs free energy density (ΔG) (figure 9a) and the phase diagram (figure 9b) has been constructed, using $v_0 = 77.4 \text{ cm}^3 \cdot \text{mol}^{-1}$ (DMF volume molar), $n=23$ (corresponding to a representative copolymer chain with 23 monomers with the following relation: 19 monomers of VDF and 4 monomers of CTFE) and the Hansen solubility parameters, $\delta = 3.31$ determined with the Blends software including in Material Studio Modeling software. This solubility parameter indicates the strong interaction between the DMF molecule and the PVDF-CTFE chain.

The Flory-Huggins theory adopted for the calculation is the extended theory that is found in Materials Studio software. The extended Flory-Huggins theory introduces two new issues and combines the Flory-Huggins model and

molecular simulation to calculate the miscibility of polymer solutions. The first one, consist on the interaction parameter, taking into consideration also the variation with temperature. The second issue, is an off-lattice calculation, this means that molecules are not distributed as a regular lattice, as they are in the conventional Flory-Huggins theory. The simulation generates thus multiple possible molecular pairs and calculate for each one, the coordination number. These computer simulations are carried out taking into account pair interactions but later there is a normalization process taking into account the interactions with the other molecules within the box. In the calculations, interactions between neighboring cells are also taken into account. More information on these issues can be found in ^{46,47}. This extension of the Flory-Huggins model is needed in order to obtain a suitable theoretical representation of the experimental results.

The variation of the free energy of mixing (ΔG) as a function of polymer concentration in the

PVDF-CTFE/DMF system is shown in figure 9a) for different evaporation temperature.

The miscibility ($\Delta G < 0$) of the system increases with increasing temperature ⁴⁸ and is affected by specific interactions between polymer and solvent and the polymer molecular weight. This behavior of miscibility is dependent on the polymer concentration for low temperatures and becomes independent of the initial polymer concentration for temperatures above 80°C.

Figure 9b) shows the phase diagram of the PVDF-CTFE/DMF system in which the three main regions -stability, metastability and instability- of the polymer solution are observed.

These regions are separated by the binodal and the spinodal lines illustrated in figure 9b). In this way, the phase separation process of the PVDF-CTFE/DMF system and therefore the resulting sample microstructure can be controlled through the initial polymer concentration and the solvent evaporation temperature.

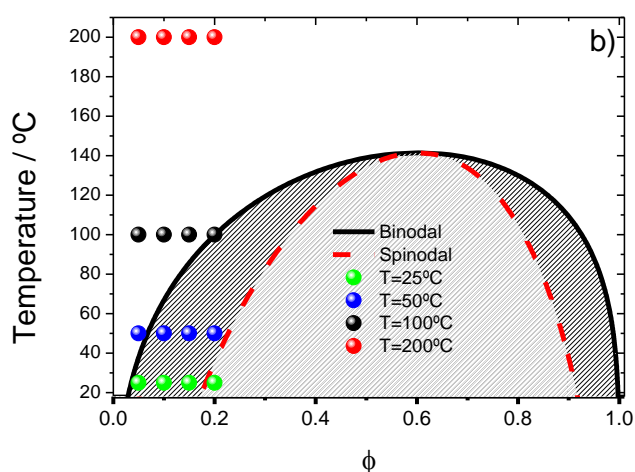
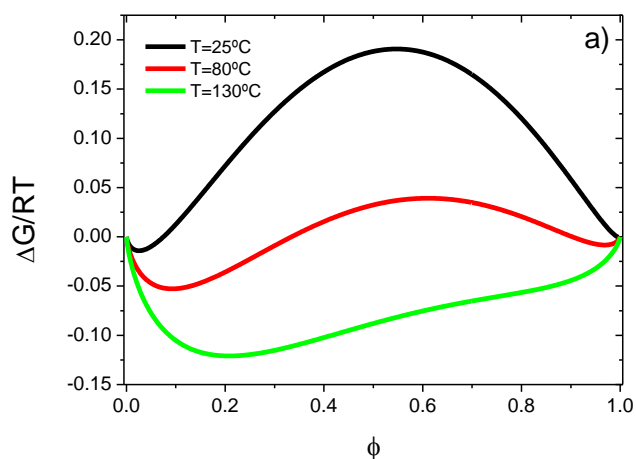


FIGURE 9 a) Variation of the Gibbs free energy and b) phase diagram for the PVDF-CTFE/DMF system.

The initial sample preparation conditions (polymer concentration and solvent evaporation temperature) are represented in the phase diagram of figure 9b) by the circles.

As represented in figure 9a) at 25°C for the different polymer/solvent ratios, the microstructure formation of the PVDF-CTFE membranes is dominated by nucleation and growth, as samples are located in the metastable region (region between the spinodal and binodal lines).

This phase separation process, leading later to morphology formation, is simulated for the PVDF-CTFE/DMF phase diagram at 25°C in figure 10a) and b). The simulated phase separation is represented by the color-codes representing the variation of the density on the system (polymer/solvent) in which red represents a higher density and blue a lower density.

Thus, simulations at 25 °C show a microphase separation where the phase separation occurs. The microphase separation (figure 10a) is lower in the more diluted solution and increases with

increasing polymer concentration in the PVDF-CTFE/DMF system (figure 10b).

Taking this fact into account, the PVDF-CTFE membranes result in final microstructures with different degree of porosity (figure 2).

For a given polymer/solvent ratio (20/80) at different solvent temperatures (25 °C, 50°C, 100°C and 100 °C) the system passes from the metastable region to the one-phase region (homogeneous microstructure) above 100°C and no porous microstructure is observed (figure 2). This fact is also observed in the simulated initial morphology (figure 10c) and d)).

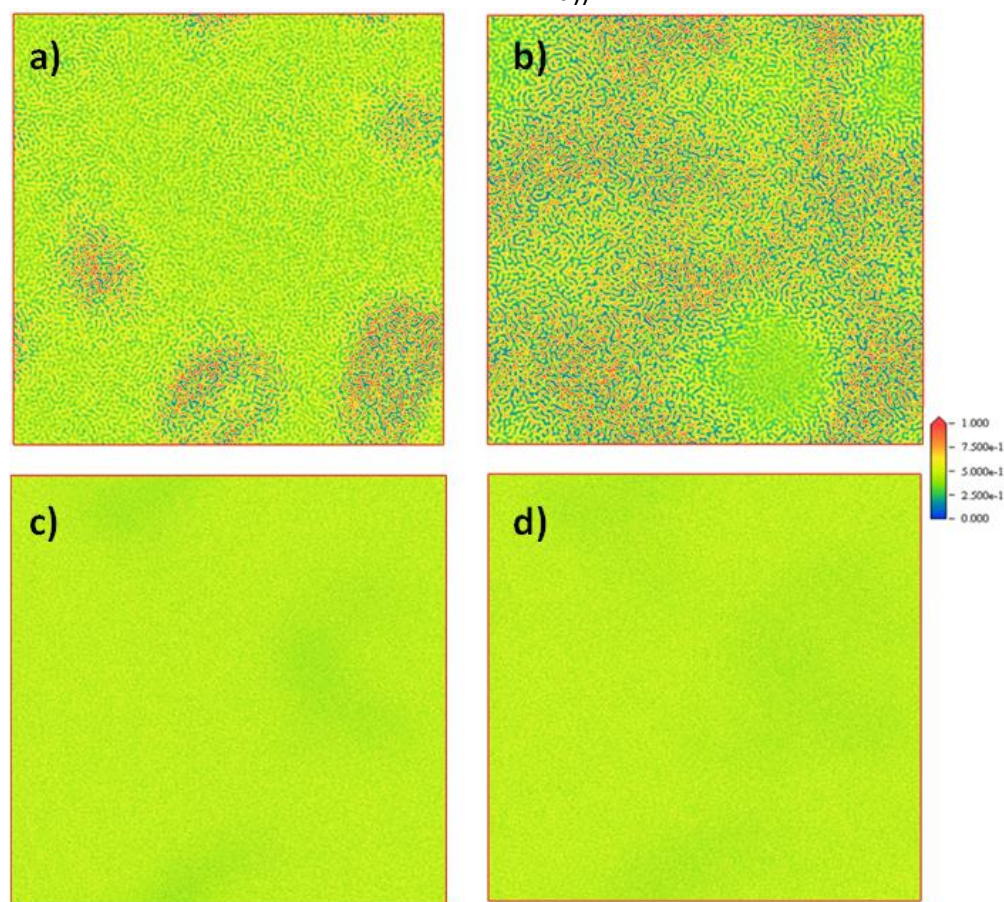


FIGURE 10 Representation of the PVDF-CTFE structure in the PVDF-CTFE/DMF system at 25°C for a) 5% of PVDF-CTFE and b) 20% of PVDF-CTFE and at 200°C for c) 5% of PVDF-CTFE and d) 20% of PVDF-CTFE in the initial solution. The color-code represent the variation of the density on the system (polymer/solvent) in which red represent a higher density a blue a lower density.

For high evaporation temperature (200°C), independently of the polymer concentration, the sample preparation conditions are located

outside the binodal line and no liquid-liquid phase separation is observed (figure 10c) and d)).

Finally, the factor that affects more the phase separation, observed in figure 10, is the solvent evaporation temperature in comparison with polymer concentration, within the ranges used in the present investigation.

The β -phase content, thermal, mechanical, dielectric and piezoelectric properties of PVDF-CTFE samples depend on the initial polymer concentration and solvent evaporation temperature, as shown in figures 4, 5, 6, 7 and 8, respectively.

At room temperature, the degree of porosity of PVDF-CTFE membranes depends on the polymer concentration as is illustrated in the figure 2. The β -phase content of PVDF-CTFE membranes depends more on solvent evaporation temperature than on polymer concentration (figure 4). The maximum β -phase fraction (87%) was determined for 20 wt% initial polymer concentration at a solvent evaporation temperature of 100°C.

The differences observed in the degree of crystallinity (values between 15% and 27%) (figure 4 and table 3) for all PVDF-CTFE membranes, are ascribed to the deferral of liquid-liquid demixing process and correlated to the phase separation and solvent evaporation rate influenced by thermodynamic parameters (affinity) and kinetics factors (molar volumes). The Young's modulus and yielding stress depend on the evaporation solvent temperature and polymer concentration as they are mainly affected by the degree of crystallinity.

Finally, the dielectric and piezoelectric properties of PVDF-CTFE membranes are correlated mainly with the β -phase content (figure 7 and 8, respectively).

CONCLUSIONS

The influence of polymer/solvent ratio and solvent evaporation temperature in the microstructure and physic-chemical properties of poly(vinylidene fluoride-co-chlorotrifluoroethylene) PVDF-CTFE membranes prepared by solvent casting is evaluated.

PVDF-CTFE membranes have been prepared with a wide-range of different morphologies. The porous microstructure of the PVDF-CTFE membranes is attributed to spinodal decomposition of the liquid-liquid phase separation.

These microstructures are correlated through the phase diagrams for the binary system (PVDF-CTFE/DMF system) obtained by the Flory-Huggins theory assuming random mixing of chains in the calculation of the entropy and segments in the calculation of the enthalpy. For PVDF-CTFE membranes, the β -phase content, thermal, mechanical, dielectric and piezoelectric properties depends on the initial polymer concentration and solvent evaporation temperature. We argue that PVDF-CTFE membranes with different morphologies, thermal, dielectric and piezoelectric properties are suitable for their use in different applications from sensor and actuator to different membrane technologies.

ACKNOWLEDGEMENTS

This work is funded by FEDER funds through the "Programa Operacional Factores de Competitividade – COMPETE" and by national funds from FCT – Fundação para a Ciência e a Tecnologia, in the framework of the strategic project Strategic Project PEST-C/FIS/UI607/2014 and PEST-C/QUI/UI0686/2013). The authors also thank funding from Matepro –Optimizing Materials and Processes", ref. NORTE-07-0124-FEDER-000037", co-funded by the "Programa Operacional Regional do Norte" (ON.2 – O Novo Norte), under the "Quadro de Referência Estratégico Nacional" (QREN), through the "Fundo Europeu de Desenvolvimento Regional" (FEDER), and grant SFRH/BD/68499/2010 (C.M.C.). The authors thank Solvay for kindly supplying the high quality materials and the Departamento de Química Física, Facultad de Ciencia y Tecnología, Universidad del País Vasco UPV/EHU, Spain, for hosting a research stay in which the theoretical work was performed.

REFERENCES AND NOTES

1. Cui, Z.; Drioli, E.; Lee, Y. M. *Progress in Polymer Science* 2014, 39, 164-198.
2. Tan, S.; Li, J.; Gao, G.; Li, H.; Zhang, Z. *Journal of Materials Chemistry* 2012, 22, 18496-18504.
3. Singh, A.; Soni, P. K.; Shekharam, T.; Srivastava, A. *Journal of Applied Polymer Science* 2013, 127, 1751-1757.
4. Li, Z.; Wang, Y.; Cheng, Z.-Y. *Applied Physics Letters* 2006, 88, -.
5. Liu, F.; Abed, M. R. M.; Li, K. *Chemical Engineering Science* 2011, 66, 27-35.
6. Jarvis, C. R.; Macklin, A. J.; Teagle, D. A.; Cullen, J.; Macklin, W. J. *Journal of Power Sources* 2003, 119-121, 465-468.
7. Ameduri, B. *Chemical Reviews* 2009, 109, 6632-6686.
8. Lovinger, A. J. *Science* 1983, 220, 1115-1121.
9. Kim, R. H.; Kang, S. J.; Bae, I.; Choi, Y. S.; Park, Y. J.; Park, C. *Organic Electronics* 2012, 13, 491-497.
10. Amirinejad, M.; Madaeni, S. S.; Navarra, M. A.; Rafiee, E.; Scrosati, B. *Ionics* 2010, 16, 681-687.
11. Lee, H.; Alcoutlabi, M.; Watson, J. V.; Zhang, X. *Journal of Polymer Science Part B: Polymer Physics* 2013, 51, 349-357.
12. Lee, H.; Alcoutlabi, M.; Watson, J. V.; Zhang, X. *Journal of Applied Polymer Science* 2013, 129, 1939-1951.
13. Buckley, G. S.; Roland, C. M.; Casalini, R.; Petchsuk, A.; Chung, T. C. *Chemistry of Materials* 2002, 14, 2590-2593.
14. Lee, H.; Alcoutlabi, M.; Toprakci, O.; Xu, G.; Watson, J.; Zhang, X. *Journal of Solid State Electrochemistry* 2014, 1-8.
15. Zhang, M.; Russell, T. P. *Macromolecules* 2006, 39, 3531-3539.
16. California, A.; Cardoso, V. F.; Costa, C. M.; Sencadas, V.; Botelho, G.; Gómez-Ribelles, J. L.; Lanceros-Mendez, S. *European Polymer Journal* 2011, 47, 2442-2450.
17. Dargaville, T. R.; Celina, M.; Chaplya, P. M. *Journal of Polymer Science Part B: Polymer Physics* 2005, 43, 1310-1320.
18. Petschek, R. G.; Metiu, H. *The Journal of Chemical Physics* 1983, 79, 3443-3456.
19. Altevogt, P.; Evers, O. A.; Fraaije, J. G. E. M.; Maurits, N. M.; van Vlimmeren, B. A. C. *Journal of Molecular Structure: THEOCHEM* 1999, 463, 139-143.
20. Lin, D.-J.; Chang, C.-L.; Huang, F.-M.; Cheng, L.-P. *Polymer* 2003, 44, 413-422.
21. Pinna, I.; Koros, W. J. *Journal of Polymer Science Part B: Polymer Physics* 1993, 31, 419-427.
22. Magalhães, R.; Durães, N.; Silva, M.; Silva, J.; Sencadas, V.; Botelho, G.; Gómez Ribelles, J. L.; Lanceros-Méndez, S. *Soft Materials* 2010, 9, 1-14.
23. Wang, X.; Zhang, L.; Sun, D.; An, Q.; Chen, H. *Desalination* 2009, 236, 170-178.
24. Ma, W.; Yuan, H.; Wang, X. *Membranes* 2014, 4, 243-256.
25. Dietz, P.; Hansma, P. K.; Inacker, O.; Lehmann, H.-D.; Herrmann, K.-H. *Journal of Membrane Science* 1992, 65, 101-111.
26. Martins, P. M.; Ribeiro, S.; Ribeiro, C.; Sencadas, V.; Gomes, A. C.; Gama, F. M.; Lanceros-Mendez, S. *RSC Advances* 2013, 3, 17938-17944.
27. Han, R.; Jin, J.; Khanchaitit, P.; Wang, J.; Wang, Q. *Polymer* 2012, 53, 1277-1281.
28. Martins, P.; Lopes, A. C.; Lanceros-Mendez, S. *Progress in Polymer Science* 2014, 39, 683-706.

29. Boschet, F.; Ameduri, B. *Chemical Reviews* 2013, 114, 927-980.
30. Yang, X.; Li, Z.; Odum, L.; Cheng, Z.-Y. *MRS Online Proceedings Library* 2005, 889, null-null.
31. Gregorio, J. R.; Cestari, M. *Journal of Polymer Science Part B: Polymer Physics* 1994, 32, 859-870.
32. Chinaglia, D. L.; Gregorio, R.; Stefanello, J. C.; Pisani Altafim, R. A.; Wirges, W.; Wang, F.; Gerhard, R. *Journal of Applied Polymer Science* 2010, 116, 785-791.
33. Gee, R. H.; Fried, L. E.; Cook, R. C. *Macromolecules* 2001, 34, 3050-3059.
34. Marega, C.; Marigo, A. *European Polymer Journal* 2003, 39, 1713-1720.
35. Olabis, O. *Polymer-Polymer Miscibility*; Elsevier Science, 2012.
36. Zhang, M.; Zhang, A.-Q.; Zhu, B.-K.; Du, C.-H.; Xu, Y.-Y. *Journal of Membrane Science* 2008, 319, 169-175.
37. Ward, I. M.; Sweeney, J. *An Introduction to the Mechanical Properties of Solid Polymers*; Wiley, 2004.
38. Sencadas, V.; Lanceros-Méndez, S.; Sabater i Serra, R.; Andrio Balado, A.; Gómez Ribelles, J. L. *The European Physical Journal E* 2012, 35, 1-11.
39. Xiao, J.; Zhou, X.; Zhang, Q. M.; Dowben, P. A. *Journal of Applied Physics* 2009, 106, -.
40. Arisawa, H.; Yano, O.; Wada, Y. *Ferroelectrics* 1981, 32, 39-41.
41. Kremer, F.; Sch?nhals, A. *Broadband Dielectric Spectroscopy*; Springer Berlin Heidelberg, 2003.
42. Dyre, J. C. *Journal of Applied Physics* 1988, 64, 2456-2468.
43. Gomes, J.; Nunes, J. S.; Sencadas, V.; Lanceros-Mendez, S. *Smart Materials and Structures* 2010, 19, 065010.
44. Wise, D. L. *Electrical and Optical Polymer Systems: Fundamentals: Methods, and Applications*; Taylor & Francis, 1998.
45. Rubinstein, M.; Colby, R. H. *Polymer Physics*; OUP Oxford, 2003.
46. Fan, C.F.; Olafson, B.D.; Blanco, M.; Hsu, S. L. *Macromolecules* 1992, 25, 3667-3676.
47. Blanco, M. J. *J. Comput. Chem.* 1991, 12, 237-247.
48. Robeson, L. M. *Polymer Blends: A Comprehensive Review*; Hanser, 2007.

GRAPHICAL ABSTRACT

Ricardo E. Sousa, José Carlos C. Ferreira, Carlos. M. Costa, Ana V. Machado, Maria M. Silva, Senentxu Lanceros-Mendez

TAILORING POLY(VINYLIDENE FLUORIDE – CO - CHLOROTRIFLUOROETHYLENE) MICROSTRUCTURE AND PHYSICO-CHEMICAL PROPERTIES BY EXPLORING ITS BINARY PHASE DIAGRAM WITH DIMETHYLFORMAMIDE

TEXT

Poly(vinylidene fluoride-co-chlorotrifluoroethylene), PVDF-CTFE, membranes that are used in different applications such as, sensors, actuators, battery separators and the variations of its microstructure have been investigated as a function of polymer concentration and evaporation solvent temperature. These microstructures are correlated through the phase diagrams for the binary system (PVDF-CTFE/DMF system) obtained by the Flory-Huggins theory. For PVDF-CTFE membranes, the β -phase content, thermal and mechanical properties depend on the initial polymer concentration and solvent evaporation temperature.

GRAPHICAL ABSTRACT FIGURE

